Mean-field free-energy approach to the lattice Boltzmann method for liquid-vapor and solid-fluid interfaces

Junfeng Zhang, Baoming Li, and Daniel Y. Kwok*
Nanoscale Technology and Engineering Laboratory, Department of Mechanical Engineering, University of Alberta, Edmonton, Alberta, Canada T6G 2G8
(Received 31 May 2003; published 31 March 2004)

We present a lattice Boltzmann method (LBM) using a mean-field representation of the free energy for fluid systems. This free-energy approach provides more realistic contact angles and fluid density profiles near the vicinity of an impenetrable wall which cannot be easily obtained by other LBM schemes. Our method was tested against various criteria and the results are in good agreement with those from thermodynamics and molecular dynamics considerations. This mean-field approach to LBM can have an important implication on studies where the solid-fluid interactions are crucial to fluidic behaviors.

DOI: 10.1103/PhysRevE.69.032602 PACS number(s): 68.08.−p, 68.03.Cd, 47.11.+j, 05.70.Np

The lattice Boltzmann method (LBM) has experienced tremendous development in simulating fluid hydrodynamic behaviors for the past decade [1–4]. When compared with traditional computational fluid dynamic methods, LBM has the advantage that numerical algorithms can be easily implemented with complex solid or free boundaries even for multiphase systems [1,5]. It should be noted that most of the existing LBM schemes can only simulate phase separation and interface formation phenomenologically. These methods, however, typically produce significant spurious currents within the interfacial region even at equilibrium [5–10].

Swift *et al.* were among the first to employ a thermodynamic free-energy approach for the LBM scheme in modeling isothermal systems with liquid-vapor interfaces or with two mutually interacting fluids [9,11]. Others have also employed this and similar free-energy models to simulate various hydrodynamic systems [5,8,12]. In Swift's model, free energy was expressed by a square-gradient expression of the van der Waals theory using Cahn-Hilliard description of nonequilibrium dynamics [5,13]. In reality, however, the presence of an impenetrable solid boundary imposes a discontinuity on the local fluid density near the wall. Thus, the gradient expansion approximation used in deriving the square-gradient theory is inadequate for description of solid-fluid interfaces [14,15]. As a result, meaningful fluid dynamics simulations by LBM involving solid-fluid interfaces often require adjustment of interaction parameters which might not truly reflect the physics of specific solid-fluid systems.

Since solid-fluid interactions play a vital role in interfacial phenomena for micro/nanofluidics [16,17], dynamic wetting [18], and thin liquid film stability [19], we propose a free-energy approach to the LBM by means of a mean-field representation. This mean-field representation has very recently been employed by us and others to study various wetting and adhesion phenomena [14,20,21]. We will illustrate below that our LBM simulations are in good agreement with those obtained from thermodynamics and molecular dynamics (MD).

*Author to whom correspondence should be addressed.
Tel: (780) 492-2791. Fax: (780) 492-2200.
Electronic address: daniel.y.kwok@ualberta.ca

According to the mean-field approximation of van der Waals theory [14,20,22], the total free energy for a fluid system can be expressed as

$$F=\int d\mathbf{r}\left\{ \psi[\rho(\mathbf{r})]+\frac{1}{2}\rho(\mathbf{r})\int d\mathbf{r}'\,\phi_{ff}(\mathbf{r}'-\mathbf{r})[\rho(\mathbf{r}')-\rho(\mathbf{r})] + \rho(\mathbf{r})V(\mathbf{r})\right\}, \quad (1)$$

where $\psi(\rho)$ is a local free energy with respect to the bulk phase with density ρ. The second term is a nonlocal term taking into account the free-energy cost of variations in the density. $\phi_{ff}(\mathbf{r}'-\mathbf{r})$ is the interaction potential between two particles located at $\mathbf{r}'$ and $\mathbf{r}$. This term can be reduced to that of the square-gradient approximation when the local density varies slowly [14,15]. The third term represents contribution of external potential energy $V(\mathbf{r})$ to the free-energy function F. Both integrations in Eq. (1) are taken over the entire space.

With this expression of free energy, we followed the procedures described in Ref. [23] and defined the nonlocal pressure as

$$P(\mathbf{r})=\rho(\mathbf{r})\psi'[\rho(\mathbf{r})]-\psi[\rho(\mathbf{r})] + \frac{1}{2}\rho(\mathbf{r})\int d\mathbf{r}'\,\phi_{ff}(\mathbf{r}'-\mathbf{r})[\rho(\mathbf{r}')-\rho(\mathbf{r})]. \quad (2)$$

For a bulk fluid with uniform density, the nonlocal integral term disappears and Eq. (2) reverts to the equation of state of the fluid. Here, we describe the implementation of these results into a LBM algorithm. Generally, after discretization in time and space, the lattice Boltzmann equation (LBE) with a Bhatnagar-Gross-Krook collision term can be written as

$$f_i(\mathbf{x}+\mathbf{e}_i,t+1)-f_i(\mathbf{x},t)=-\frac{1}{\tau}[f_i(\mathbf{x},t)-f_i^{eq}(\mathbf{x},t)], \quad (3)$$

where the distribution function $f_i(\mathbf{x},t)$ denotes particle population moving in the direction of $\mathbf{e}_i$ in a lattice site $\mathbf{x}$ and at a time step t, τ is the collision time, and $f_i^{eq}(\mathbf{x},t)$ is a prescribed equilibrium distribution function with

$$f_0^{eq}=\rho\left[d_0-\frac{1}{c^2}\mathbf{u}^2\right],$$

$$f_i^{eq}=\rho\left[\frac{1-d_0}{b}+\frac{D}{c^2 b}\mathbf{e}_i\cdot\mathbf{u}+\frac{D(D+2)}{2c^4 b}(\mathbf{e}_i\cdot\mathbf{u})^2-\frac{D}{2bc^2}\mathbf{u}^2\right],\quad i=1,\ldots,b \tag{4}$$

for a D-dimensional lattice with b links, where the particle speed is $|\mathbf{e}_i|=c$. The constant d_0 is the equilibrium fraction of particles at rest [7]. The macroscopic density ρ and velocity $\mathbf{u}$ can be calculated from the distribution function f_i given by

$$\rho=\sum_i f_i,\quad \rho\mathbf{u}=\sum_i f_i\mathbf{e}_i. \tag{5}$$

However, if an external force $\mathbf{F}(\mathbf{x},t)$ exists, we can modify Eq. (5) to reflect the momentum change as

$$\rho\mathbf{u}=\sum_i f_i\mathbf{e}_i+\tau\mathbf{F} \tag{6}$$

and use $\mathbf{u}$ produced here to calculate the equilibrium distribution function f_i^{eq} in Eq. (4) [7,8]. Redefining the fluid momentum $\rho\mathbf{v}$ to be an average of the momentum before collision $\Sigma_i f_i\mathbf{e}_i$, and that after collision [$\rho\mathbf{u}$ in Eq. (6)] and following the Chapman-Enskog procedures, a Navier-Stokes equation with the equation of state

$$P=\frac{c^2(1-d_0)}{D}\rho+\Phi \tag{7}$$

can be obtained, where Φ is a potential energy field related to $\mathbf{F}$ by

$$\mathbf{F}(\mathbf{x},t)=-\nabla\Phi(\mathbf{x},t). \tag{8}$$

In order to obtain the Navier-Stokes equation with a pressure term similar to that given by Eq. (2), we set an artificial Φ as follows:

$$\Phi(\mathbf{x},t)=\rho(\mathbf{x})\psi'[\rho(\mathbf{x})]-\psi[\rho(\mathbf{x})]+\frac{1}{2}\rho(\mathbf{x})\int d\mathbf{x}'\,\phi_{ff}(\mathbf{x}'-\mathbf{x})[\rho(\mathbf{x}')-\rho(\mathbf{x})]-\frac{c^2(1-d_0)}{D}\rho(\mathbf{x}). \tag{9}$$

The above equations setup a complete LBM scheme with the mean-field free-energy function implemented. To verify its correctness and demonstrate its applicability, we adopt a van der Waals fluid model

$$\psi(\rho)=\rho kT\ln\frac{\rho}{1-b\rho}-a\rho^2, \tag{10}$$

where a and b are the van der Waals constants, k is the Boltzmann constant, and T is the absolute temperature. In a lattice grid, the interaction potential ϕ_{ff} can be reduced to a single number K [7],

$$\phi_{ff}(\mathbf{x}'-\mathbf{x})=\begin{cases}K, & |\mathbf{x}'-\mathbf{x}|=c\\ 0, & |\mathbf{x}'-\mathbf{x}|\neq c,\end{cases} \tag{11}$$

which measures the interaction strength among the nearest neighboring particles. Thus, the nonlocal integral term can be replaced by a summation over its neighbors of a site $\mathbf{x}$. In the following simulations, we selected $a=9/49$, $b=2/21$, $kT=0.55$, $\tau=1.0$, and $K=-0.01$, unless otherwise stated, a negative K implies that the interaction is attractive. A D2Q7 lattice is employed, for which $D=2$, $b=6$, $d_0=1/2$, $c=1$, $\mathbf{e}_0=[0,0]$, and $\mathbf{e}_i=[\cos\pi(i-1)/3,\ \sin\pi(i-1)/3]$ ($i=1,\ldots,6$) in Eq. (4).

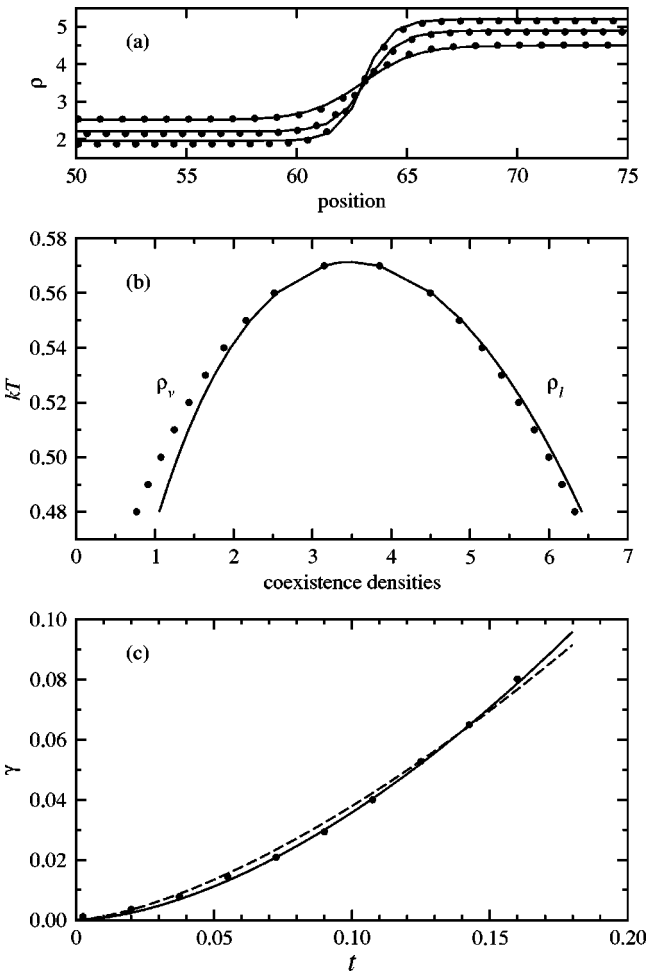

FIG. 1. (a) Density distributions across liquid-vapor interfaces, (b) coexistence densities of liquid/vapor phases, and (c) liquid-vapor interfacial tensions at different temperatures.

It should be noted that having the ability to generate a reasonable liquid-vapor interface is crucial for any multiphase models. We tested our model using a simulation lattice configuration of a size 128×128, with a nonuniform initial density distribution, zero initial velocity, and periodic boundary conditions. The data shown in Fig. 1 were obtained after 10 000 time steps with a velocity in the interfacial region of the order of 10^{-5}. Figure 1(a) shows the density profiles

across a liquid-vapor interface at different temperatures. The solid curves are not curve fits but the theoretical results by minimizing the total free energy in Eq. (1). In Fig. 1(b), we also plotted the coexistence liquid and vapor densities with temperatures. Our LBM simulation data are represented by symbols and those by a Maxwell construction by solid curves. It is apparent that our LBM simulation results for liquid-vapor interfaces are in good agreement with theoretical predictions based on free-energy expressions. As temperature decreases from the critical temperature T_c, the interfacial thickness decreases with a sharper interface. This can introduce significant errors into the LBM simulation because of a finite lattice length. Such an effect can be seen in Figs. 1(a) and 1(b). Similar difficulties also occur in other multiphase/multicomponent LBM models [6,7,9]. Knowing the density distribution across a liquid-vapor interface, we can easily calculate the interfacial tension γ by integrating the excess free energy across the interfacial region [20,21]. The results are displayed in Fig. 1(c) versus the reduced temperature $t=(T_c-T)/T_c$. Fitting the data with a function of the form $\gamma=\alpha t^{\beta}$ gives $\beta=1.68$ (solid curve), while the mean-field theory predicts $\beta=1.5$ [24]. A fitting of $\gamma=\alpha t^{1.5}$ to our data is also shown as a dashed curve. It is apparent in Fig. 1 that our LBM simulation results for liquid-vapor interfaces agree well with those of thermodynamics.

Our next illustration is by means of the bubble test to examine a multiphase/multicomponent models [7,9,10]. In our simulations, we setup a rectangular high-density region in the center of a 128×128 lattice domain with periodic boundary conditions. After 10 000 time steps, the system reached equilibrium and formed a circular liquid bubble. Figure 2(a) shows the density distribution versus the distance from the bubble center. It should be noted that nearly all points lie on a single curve. The variation from the single curve is estimated to be about one lattice length, suggesting that this model has a very good isotropy. By measuring the bubble radius R and the pressures inside/outside of the bubble, P_{in} and P_{out}, the Laplace equation of capillarity

$$P_{in}-P_{out}=\gamma/R \tag{12}$$

can be verified. It is clear from Fig. 2(b) that the numerical results follow Eq. (12) very closely. A linear curve fitting yielded a slope of 6.4×10^{-3} and is similar to that calculated from Fig. 1 using density profile (7.8×10^{-3}). The Galilean invariance is another important property for LBM models, since the system behavior should be invariant even when the reference coordinates are being translated at any given constant velocity. The data in Fig. 2(c) were obtained by setting different initial horizontal velocity U for the reference coordinates and measuring the corresponding liquid bubble size, radii in horizontal r_h, and vertical direction r_v. Clearly, the bubble behaves as a perfect circle and does not change with the reference velocity U. These results suggest that our model is indeed better than the original one by Swift *et al.* [11] and is comparable to the modified one [12] with respect to the Galilean invariance.

Given that the simulations for liquid-fluid interfacial properties have been verified, we focus our attention here on

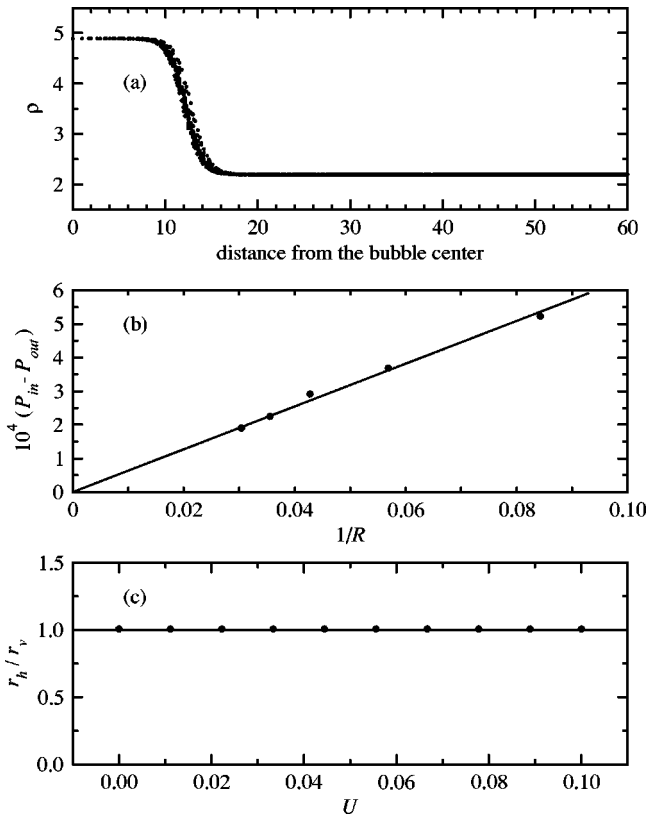

FIG. 2. (a) Density distribution against the distance from the bubble center, (b) pressure differences across the bubble interface of different bubble sizes, and (c) ratio of the two radii at perpendicular directions when the reference system moves at U.

the solid-fluid interfaces. The strength of our mean-field LBM is in its ability to study solid-fluid interface. In the following demonstration, an exponentially decaying potential was used to model the solid wall effects upon the fluid,

$$V(\mathbf{r})=-K_w\exp(-h/c), \tag{13}$$

where K_w is the attraction strength and h is the distance from the wall at point $\mathbf{r}$. For a 128×128 lattice domain, the bottom layer sites are applied with a general bounce-back boundary condition, while a mirror boundary condition is applied at the top layer sites. The left and right ends are still given by the periodic boundary conditions. By adjusting the wall attraction strength K_w, we can generate different contact angles θ, from complete wetting to complete dewetting, as illustrated in Fig. 3. The contact angle is found to be almost a linear function of K_w and is in agreement with the results from other independent studies [25,26]. We wish to point out that, unlike other models [25,27], a contact angle value between 0° and 180° can be generated without using a repulsive solid-fluid interaction. This is consistent with MD simulations [28,29] and physical reality.

Figure 4 shows the density distributions of a bulk fluid against a wall with different attraction strengths. We found that there is always a dryer (low-density) layer between the bulk liquid and the wall. This result is consistent with thermodynamic considerations [20] and MD simulations [28,29].

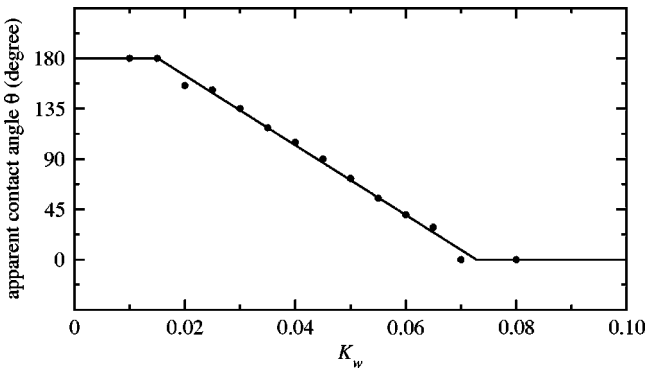

FIG. 3. The apparent contact angles θ as a function of solid-fluid attraction strengths K_w.

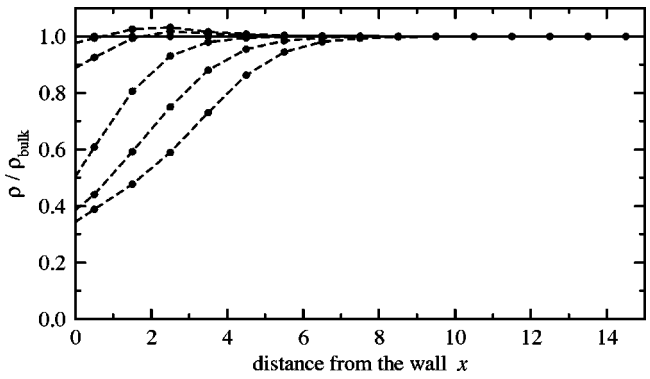

FIG. 4. The fluid density distributions near an impenetrable wall for different interaction strength, $K_w = 0.00$, 0.02, 0.04, 0.06, and 0.08 (from bottom to top). The solid line is the corresponding distribution from a standard LBM method.

Nevertheless, the density profiles show no oscillatory behavior near the wall as found from MD results. This is due to the fact that short-ranged interactions have been neglected in our approximation [14,20]. In Fig. 4, the solid straight line is the density profile from a standard D2Q7 LBM simulation. Clearly, without using the free-energy approach described here, a standard D2Q7 has failed to predict the density variation near the wall.

In conclusion, we have applied a mean-field approximation of free energy to the lattice Boltzmann method. The contribution of this model more important than previous work is that solid-fluid boundary effects are considered thermodynamically in a more realistic case. As a result, more reasonable contact angles and fluid density profiles near a solid wall can be obtained. Our simulation results agree well with those predicted by thermodynamics and molecular dynamics, suggesting that our mean-field approach to LBE for liquid-vapor and solid-fluid interfaces might have important implications on studies where solid-fluid interactions are crucial to fluidic behaviors.

This work was supported, in part, by the Alberta Ingenuity Establishment Fund, Canada Research Chair (CRC) Program, and Natural Sciences and Engineering Research Council of Canada (NSERC). J.Z. acknowledges financial support from the Alberta Ingenuity.

[1] S. Chen and G.D. Doolen, Annu. Rev. Fluid Mech. **30**, 329 (1998).
[2] D.A. Wolf-Gladrow, *Lattice-Gas Cellular Automata and Lattice Boltzmann Models: An Introduction* (Springer, Berlin, 2000).
[3] R. Benzi, S. Succi, and M. Vergassola, Phys. Rep. **222**, 145 (1992).
[4] S. Succi, *The Lattice Boltzmann Equation: For Fluid Dynamics and Beyond* (Oxford University Press, Oxford, U.K. 2001).
[5] A.D. Angelopoulos, V.N. Paunov, V.N. Burganos, and A.C. Payatakes, Phys. Rev. E **57**, 3237 (1998).
[6] C. Appert, D.H. Rothman, and S. Zaleski, Physica D **47**, 85 (1991).
[7] X. Shan and H. Chen, Phys. Rev. E **49**, 2941 (1994).
[8] J.M. Buick, Ph. D. thesis, The University of Edinburgh, U.K., 1997 (unpublished).
[9] M.R. Swift, W.R. Osborn, and J.M. Yeomans, Phys. Rev. Lett. **75**, 830 (1995).
[10] S. Hou, X. Shan, Q. Zou, G.D. Doolen, and W.E. Soll, J. Comput. Phys. **138**, 695 (1997).
[11] M.R. Swift, E. Orlandini, W.R. Osborn, and J.M. Yeomans, Phys. Rev. E **54**, 5041 (1996).
[12] A.N. Kalarakis, V.N. Burganos, and A.C. Payatakes, Phys. Rev. E **65**, 056702 (2002).
[13] J.W. Cahn and J.E. Hilliard, J. Chem. Phys. **28**, 258 (1958).
[14] D.E. Sullivan, J. Chem. Phys. **74**, 2604 (1981).
[15] B. Widom, J. Stat. Phys. **19**, 563 (1978).
[16] B. Li and D.Y. Kwok, Phys. Rev. Lett. **90**, 124502 (2003).
[17] S. Succi, Phys. Rev. Lett. **89**, 064502 (2002).
[18] J. Coninck, M.J. Ruijter, and M. Voue, Curr. Opt. Colloid Interface Sci. **6**, 49 (2001).
[19] J.A. Diez and L. Kondic, Phys. Rev. Lett. **86**, 632 (2001).
[20] A.E. van Giessen, D.J. Bukman, and B. Widom, J. Colloid Interface Sci. **192**, 257 (1997).
[21] J. Zhang and D.Y. Kwok, J. Phys. Chem. B **106**, 12 594 (2002).
[22] J. Rowlinson and B. Widom, *Molecular Theory of Capillary* (Claredon, Oxford, 1982).
[23] A.J.M. Yang, P.D. Fleming, and J.H. Gibbs, J. Chem. Phys. **64**, 3732 (1976).
[24] A.E. van Giessen, E.M. Blokhuis, and D.J. Bukman, J. Chem. Phys. **108**, 1148 (1998).
[25] Q. Kang, D. Zhang, and S. Chen, Phys. Fluids **14**, 3203 (2002).
[26] Z.L. Yang, T.N. Dinh, R.R. Nourgaliev, and B.R. Sehgal, Int. J. Heat Mass Transfer **44**, 195 (2001).
[27] L. Fan, H. Fang, and Z. Lin, Phys. Rev. E **63**, 051603 (2001).
[28] M.J.P. Nijmeijer, C. Bruin, A.F. Bakker, and J.M.J. van Leeuwen, Phys. Rev. A **42**, 6052 (1990).
[29] J.-L. Barrat and L. Bocquet, Phys. Rev. Lett. **82**, 4671 (1999).